A&A manuscript no. (will be inserted by hand later)	ASTRONOMY
Your thesaurus codes are: 04(11.09.1; 11.09.4; 11.19.3; 13.09.1)	AND ASTROPHYSICS 19.10.2018

ISOCAM images at 6.75 μ m and 15 μ m: the circumnuclear region of NGC 4321 (M 100) *

H. Wozniak¹, D. Friedli^{2,3}, L. Martinet³, and D. Pfenniger³

- ¹ IGRAP/Observatoire de Marseille, F-13248 Marseille Cedex 4, France
- ² Département de Physique and Observatoire du Mont Mégantic, Université Laval, Québec, QC, G1K 7P4, Canada
- ³ Observatoire de Genève, CH-1290 Sauverny, Switzerland

Received 5 September 1997, accepted 18 September 1997

Abstract. We present ISOCAM images $(1.5''px^{-1})$ in the LW2 $(6.75\,\mu\text{m})$ and LW3 $(15\,\mu\text{m})$ broad band filters of the circumnuclear starburst of NGC 4321 (M 100). A detailed comparison with the emission at other wavelengths $(U, B, H\alpha, \text{ and CO})$ is also presented. The nature and intensity of the mid-infrared emission is shown to be remarkably different from one star forming region to the next. For instance, star forming regions at the ends of the nuclear bar may contain enshrouded Wolf-Rayet stars.

Key words: Galaxies: individual: NGC 4321, M 100 - Galaxies: ISM - Galaxies: starburst - Infrared: galaxies

1. Introduction

This *Letter* is a first account of a global project intended to clarify the interplay between starburst activity and the non-axisymmetric dynamics of barred galaxies (Wozniak et al. 1997).

NGC 4321 (M 100), a late-type giant, moderately barred spiral galaxy in Virgo, represents one of the best laboratories for this purpose. Its inner region has been extensively studied at several wavelengths. Optical (Pierce 1986), $\text{H}\alpha$, near-infrared (Knapen et al. 1995a,b), and CO images (Rand 1995; Sakamoto et al. 1995) have revealed many intricate features associated with its mild star formation activity in the central kpc. Several HII regions lie on a 1 kpc circumnuclear ring crossing a 8 kpc long stellar bar. A nuclear bar occupies the region inside the ring (Knapen et al. 1995a). Its almost perfect alignment

Send offprint requests to: wozniak@observatoire.cnrs-mrs.fr

with the large-scale bar may be coincidental since, as we know now, concentric bars can rotate at different speeds (Friedli & Martinet 1993). The assumed distance to M 100 is 17.1 Mpc (Freedman et al. 1994) which on the sky corresponds to $83\,\mathrm{pc}\,\mathrm{arcsec}^{-1}$.

The Infrared Space Observatory (ISO, Kessler et al. 1996) offers a unique opportunity to explore the characteristics of the mid-infrared (MIR) emission of this galaxy, in particular the emission coming from "unidentified infrared emission bands" (UIBs) and hot dust. The actual nature of the chemical species responsible for UIBs is still under debate, although PAH molecules are promising candidates. The PAHs and hot dust reemit, in the near- and mid-infrared, the absorbed ultraviolet and visible photons (Allamandola et al. 1989), justifying a multiwavelength approach to the study of star formation and dust. A spatial coincidence between dark dust lanes, visible on optical images, and hot dust emission in the MIR is expected, while the sources of exciting photons could be identified with UV images. Also, stars form in molecular clouds, well traced by CO emission. However, although a spatial association is likely to be found between CO and hot dust emission, the precise relation remains largely unclear.

Here, we focus on the characteristics of the MIR emission as well as on the spatial correlations and offsets with emission at other wavelengths.

2. ISOCAM observations and data processing

NGC 4321 was observed on 1996 July 8 with the ISO-CAM camera (Cesarsky et al. 1996) on board ISO. We used the smallest available pixel field of view (PFOV), i.e., $1.5\,\mathrm{''px^{-1}}$, which gives a $45''\times45''$ field of view. Two broad band filters were used: LW2 ($\lambda_c=6.75\,\mu\mathrm{m},\,R=\lambda_c/\Delta\lambda\approx2.25$) and LW3 ($\lambda_c=15\,\mu\mathrm{m},\,R\approx3$). The LW2 filter includes UIBs emission at $6.2\,\mu\mathrm{m},\,7.7\,\mu\mathrm{m}$ and $8.6\,\mu\mathrm{m}$ as well as the underlying continuum. The LW3 filter col-

^{*} Based on observations with instruments funded by ESA Member States (especially the PI countries: France, Germany, the Netherlands and the United Kingdom) on board ISO, an ESA project with the participation of ISAS and NASA.

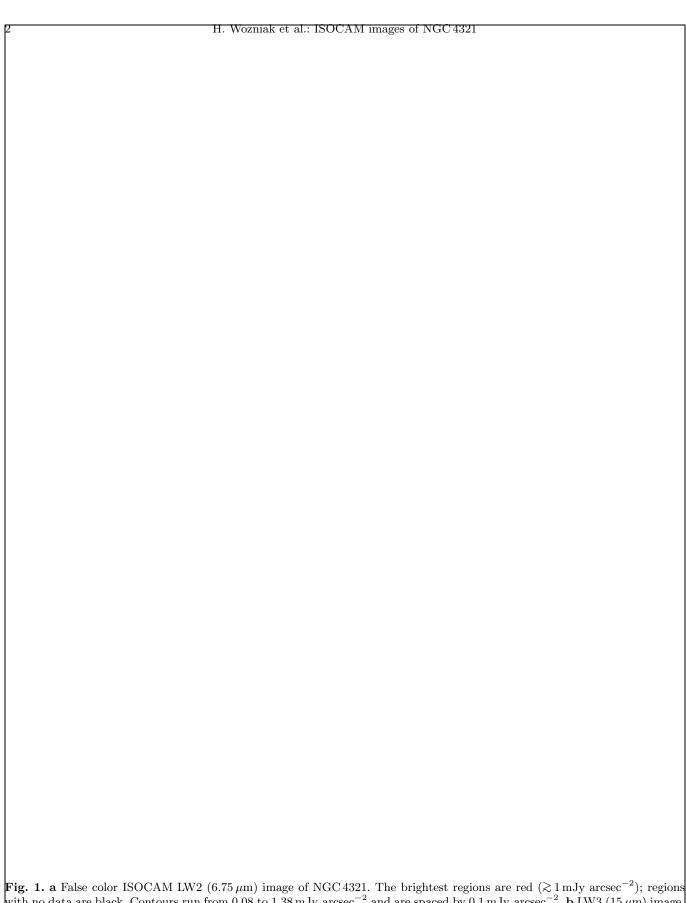


Fig. 1. a False color ISOCAM LW2 (6.75 μ m) image of NGC 4321. The brightest regions are red ($\gtrsim 1 \,\mathrm{mJy\ arcsec}^{-2}$); regions with no data are black. Contours run from 0.08 to 1.38 mJy arcsec⁻² and are spaced by 0.1 mJy arcsec⁻². b LW3 (15 μ m) image. The LW3 contours are scaled as for LW2. c LW2/LW3 colour map. Red regions have LW2/LW3>1. The huge southern black spots are an artefact. d U image with LW2 contours as in (a). The 0 mJy arcsec⁻² level is plotted as a red contour. e Hα image with LW2 contours as in (d). f CO density map with LW2 contours as in (d). All contours are red to improve readability

lects continuum emission of small grains as well as [NeII] (12.8 μ m) and [NeIII] (15.5 μ m) nebular emissions.

To remove the MIR background from our images, the beamswitching mode (AOT3) was chosen. Two empty fields 10' away from the galaxy disc were selected from IRAS maps. Each pixel on the source was exposed twice using the exposure sequence [$sky_1 \rightarrow source \rightarrow sky_2 \rightarrow source$]. Each image is composed of several hundreds of individual exposures of 2s each. Total exposure times of the resulting images are 1200s in LW2 and 720s in LW3.

The raw data were reduced with CIA, the CAM Interactive Analysis software¹, in a standard way (Cesarsky et al. 1996). We used the IAS model (Abergel et al. 1997) to correct the fluxes for transient effects. A crude estimate of the current photometric accuracy leads to a relative error of 30% (M. Sauvage, private communication). The flux lost for a point source due to the large PSF amounts to 8-16%. The resulting S/N ratios are ~ 40 at $6.75\,\mu\mathrm{m}$ and ~ 10 at $15\,\mu\mathrm{m}$.

The PSF beam FWHM is 3" at $6.75\,\mu\mathrm{m}$, and 6.3'' at $15\,\mu\mathrm{m}$. The LW2 resolution has been degraded down to that of the LW3 for computing the LW2/LW3 colour map. Our descriptions will mainly refer to the LW2 image, less affected by the PSF. We are therefore confident of detecting features larger than 3". Smaller details will require the availability of improved deconvolution algorithms.

3. Multiwavelength comparisons

Definitions. Following Knapen et al. (1995a), we label K1 and K2 the two H II regions close to nuclear bar ends (in coincidence with hot spots visible in the K-band), whereas the two strong and more extended H α regions, located near the extremities of the nuclear bar minor axis, are labeled H α 3 and H α 4 (no counterparts in K).

MIR. The LW2 and LW3 images are displayed in Figs. 1a and 1b. Both LW2 and LW3 emissions are inhomogeneous, resulting in an incomplete ring-like distribution. The two bright spots near the nuclear bar ends dominate the emission in both bands. The K1 peak is the brightest with $F_{6.75}=1.39\,\mathrm{mJy}$ arcsec⁻² but the emission displays a northern extension with $F_{6.75}\approx0.95\,\mathrm{mJy}$ arcsec⁻² on average. For the K2 spot, $F_{6.75}=1.25\,\mathrm{mJy}$ arcsec⁻². The faintest isophote which isolates the K1 and K2 regions from the rest of the ring is $0.85\,\mathrm{mJy}$ arcsec⁻². The integrated flux above this level is $71.5\,\mathrm{mJy}$ for K1 and $27.6\,\mathrm{mJy}$ for K2, while their mean surface brightnesses are similar ($\approx 1\,\mathrm{mJy}$ arcsec⁻²). This is due to the larger area of the K1 region.

Another important source is the nucleus, as bright as the K1 northern extension ($F_{6.75} = 0.94 \,\mathrm{mJy~arcsec^{-2}}$). Its integrated flux is $8 \,\mathrm{mJy}$. The mean brightness in-

side the circumnuclear ring, including the nucleus, is $F_{6.75} \approx 0.80 \,\mathrm{mJy\ arcsec^{-2}}$. No morphological differences between the LW2 and LW3 images are perceptible without deconvolution. Furthermore, the bar-like feature which seems to connect the two peaks and the nucleus remain to be confirmed with better techniques.

Naively, one might expect that the 6.75 and $15\,\mu\mathrm{m}$ emitters should be concentrated around star forming regions, or that the MIR brightness distribution should at least show similar steep gradients as for H α . The observed relative homogeneity may be due to the low map resolution, as a 1.5" pixel covers a 125 pc wide region. Alternatively, this may mean that UIBs and the underlying MIR continuum (5 – 17 $\mu\mathrm{m}$) are observed everywhere. Indeed, Mattila et al. (1996) detected the UIBs in the galactic disc where the radiation field is 10^2-10^3 lower than in H II regions or planetary nebulae. Observations of spiral galaxies (e.g. M 51, Sauvage et al. 1996; NGC 6946, Malhotra et al. 1996) also show continuum emission from the whole discs.

The LW2/LW3 colour map (Fig. 1c) shows specific patterns: the nuclear bar ends are dominated by the LW2 emission (LW2/LW3 $\approx 1.1-1.2$) while the other two HII regions are marginally dominated by LW3 emission $(LW2/LW3 \approx 0.95)$. Inside the circumnuclear ring, the LW2/LW3 ratio is lower (≈ 0.8). Thus, in the same object and over a roughly similar area (circumnuclear region), we have found star forming regions with very different MIR properties. Two interpretations of this ratio can be put forward. 1) The $6.75 \,\mu\mathrm{m}$ excess at the K1/2 peaks could be due to the circumstellar amorphous carbon dust present around Wolf-Rayet stars, especially WCs. ISO SWS spectra show a large bump peaking at $7.7 \,\mu\mathrm{m}$ (van der Hucht et al. 1996). A few tens of such massive stars could account for the LW2 excess over the LW3 emission. Moreover, their bright C IV 2.08 μ m and C III 2.11 μ m emission blends could be responsible for the K-spots (Figer et al. 1997). Thus, K1/2 starburst regions could be very young $(\lesssim 3-5\,\mathrm{Myr})$. 2) In strong radiation fields, UIBs are less intense because of the destruction of small molecules (Zavagno et al. 1992). This may be the case in the H α 4 region which is the brightest source in the U-band. The 15 μ m emission could moreover be lower at the nuclear bar ends (K1/2 regions) because the species responsible for the continuum emission are less excited. Together, these effects could explain the colour map variations.

UV. A roughly 1.1" resolution U-band image, taken with the 2.3 m telescope at Kitt Peak Observatory, was kindly provided by F. Bresolin (Bresolin & Kennicutt 1997). It shows several bright knots along the circumnuclear ring, but also a few peaks inside the ring. Figure 1d shows that the LW2 peaks are displaced from those in the U-band. In particular, the K2 peak is surrounded by U-bright regions. The only noticeable exceptions are the nucleus, bright in U, LW2, LW3, and a northern overlap close to $H\alpha3$.

¹ CIA is a joint development by the ESA Astrophysics Division and the ISOCAM Consortium led by the ISOCAM PI, C. Cesarsky, DSM, CEA, France.

Visible. HST images, taken with broad band filters F439W (B), F555W (V), and F702W (R), have been extracted from the Space Telescope Institute archives. The 40" central region of M 100 has been observed with the PC camera at $0.046\,\mathrm{''px^{-1}}$. A comparison between HST and ISOCAM images shows that the LW2 peaks are located in, or at the inner edge of, the dust lanes. There is also less MIR emission in the northern and southern parts of the ring as there is less dust.

 $H\alpha$. A roughly 3" resolution $H\alpha$ image, taken at Mt. Mégantic Observatory, was kindly supplied by J.-R. Roy and P. Martin. Four main regions of star formation trace a circumnuclear boxy ring with $a \approx 500 - 700 \,\mathrm{pc}$, $b/a \approx 0.75$, and oriented at a position-angle $\approx 131^{\circ}$. The comparison between H α and LW2 (Fig. 1e) shows that the K1 and K2 star forming regions are spatially associated, although a little displaced, with the LW2 peaks, while no strong counterparts to the H α 3 and H α 4 regions are visible. With respect to the nuclear bar (counter-clockwise rotation), MIR maxima are trailing, whereas $H\alpha$ ones leading. This indicates that some physical properties differ between the K1/2 and H α 3/4 regions. Moreover, a comparis on between the LW3 and H α images does not confirm the systematic connection between HII regions and LW3 peaks found by Sauvage et al. (1996). Indeed, the $H\alpha 3/4$ regions have no counterparts at $15 \,\mu m$.

CO. The $3.6''\times3.1''$ resolution CO density map of Rand (1995) is used to localize the CO spiral arms and peaks. Two molecular arms cross the bar at the location of the K1/2 regions, while the northern and southern parts are offset toward the outer edge of the $\text{H}\alpha3/4$ regions. CO interferometric maps indicate different physical properties in the K1/2 and $\text{H}\alpha3/4$ regions (Fig. 1f). On one hand, they show that the CO arms do not coincide with the $\text{H}\alpha3/4$ regions and thus, they do not coincide with the strong LW2 emission. On the other hand, the nuclear bar ends are sites of strong CO emission, roughly correlated (i.e., inside $200-300\,\text{pc}$) with the peaks in LW2, LW3, $\text{H}\alpha$, U and K-bands.

4. Main conclusions

- 1) The K1/2 regions, at the ends of the nuclear bar, show bright peaks in LW2 and LW3, H α , CO, U and K-bands located near the dust lanes. In these regions LW2/LW3>1, which may mean that UIB carriers dominate the MIR luminosity. These carriers may be amorphous carbon grains created in Wolf-Rayet stellar winds. Knapen et al. (1995a,b) suggested that these regions might be young, and powered by OB stars; while confirming this assertion, we suggest in addition the possible presence of WCs.
- 2) The $\text{H}\alpha 3/4$ regions, near the ends of the nuclear bar minor axis, are not associated with strong emission in LW2 and LW3 bands. In these regions, the hot dust probably dominates the MIR emission, since LW2/LW3<1. The

emission in $H\alpha$, U and the optical bands is strong. These regions are offset from the CO arms and associated dust lanes. They are the sites of the strongest circumnuclear $H\alpha$ emission, being perhaps less obscured by dust.

- 3) The centre does not show significantly strong emission in MIR bands. It has a low LW2/LW3 ratio (≈ 0.8) compared with the surrounding ring (≈ 0.95) or the K1/2 regions (≈ 1.1). It also emits in H α , U and CO.
- 4) There are no "holes" in the LW2 and LW3 surface brightness, i.e. some emission from UIB carriers and hot dust is observed everywhere in the central region. This may be either due to the low spatial resolution ($\approx 250\,\mathrm{pc}$ wide smoothing), or to the existence of a significant background of MIR continuum emission.

Acknowledgements. We are very grateful to the ISOCAM team at Saclay for many fruitful discussions and to J. Caplan who improved the English. We are indebted to F. Bresolin, P. Martin, R. Rand, and J.-R. Roy for having provided various data. H.W. thanks the ISO GdR (INSU) for financial supports during his visits at Saclay. The Swiss National Science Foundation (FNRS) is acknowledged for its essential supports to D.F. ("Advanced Researcher" fellowship), and L.M. and D.P. (grant).

References

Abergel A., Désert F.-X., Aussel H., 1997, IAS/CEA/SAp Techn. Rep.

Allamandola L.J., Tielens A.G.G., Barker J.R., 1989, ApJS 71,

Bresolin F., Kennicutt R.C., 1997, AJ 113, 975

Cesarsky C.J., Abergel, A., Agnese, P., et al., 1996, A&A 315, L32

Figer D.F., McLean I.S., Najarro F., 1997, ApJ 486, 420

Freedman W.L., Madore B.F, Stetson P.B., et al., 1994, ApJ 435, L31

Friedli D., Martinet L., 1993, A&A 277, 27

Kessler M.F., Steinz, J.A., Anderegg, M.E., et al., 1996, A&A 315, L27

Knapen J.H., Beckman J.E., Shlosman I., et al., 1995a, ApJ $443,\,\mathrm{L}73$

Knapen J.H., Beckman J.E., Heller C.H., Shlosman I., de Jong R.S., 1995b, ApJ 454, 623

Malhotra S., Helou G., Van Buren D., et al., 1996, A&A 315, L161

Mattila K., Lemke D., Haikala L.K., et al., 1996, A&A 315, L353

Pierce M.J., 1986, AJ 92, 285

Rand R.J., 1995, AJ 109, 2444

Sakamoto K., Okumura S., Minezaki T., Kobayashi Y., Wada K., 1995, AJ 110, 2075

Sauvage M., Blommaert J., Boulanger F., et al., 1996, A&A 315, L89

van der Hucht K.A., Morris P.W., Williams P.M., et al., 1996, A&A 315, L193

Wozniak H., Friedli D., Martinet L., Pfenniger D., 1997, in Extragalactic Astronomy in the Infrared, G.A. Mamon et al. (eds.), Editions Frontières, Gif-sur-Yvette, in press (see also astro-ph/9708137)

Zavagno A., Cox P., Baluteau J.-P., 1992, A&A 259, 241

This article was processed by the author using Springer-Verlag \LaTeX A&A style file L-AA version 3.

